Progress of Theoretical Physics, Vol. 100, No. 2, August 1998

Indicators of Reconnection Processes and Transition to Global Chaos in Nontwist Maps

Susumu SHINOHARA and Yoji AIZAWA

Department of Applied Physics, Waseda University, Tokyo 169-8555

(Received April 3, 1998)

Reconnection processes of twin-chains are systematically studied in the quadratic twist map. By using the reversibility and symmetry of the mapping, the location of the indicator points is theoretically determined in the phase space. The indicator points enable us to obtain useful information about the reconnection processes and the transition to global chaos. We succeed in deriving the general conditions for the reconnection thresholds. In addition, a new type of reconnection process which generates shearless curves is studied.

§1. Introduction

In the past decades, enormous effort has been dedicated to the study of two-dimensional area-preserving maps with the twist condition,[1] but very few studies have been made of nontwist maps. Recent studies on nontwist maps have revealed that rich properties are generated by violating the twist condition.[2)-6)]

In a previous paper,[6] we studied the properties of the quadratic twist map and numerically determined the critical boundary in the two-dimensional parameter space, where the transition to global chaos occurs. The critical boundary has many sharp singular structures, and their locations seem to have a one-to-one correspondence with those of the reconnection thresholds. The relationship between the transition to global chaos and the reconnection processes was first pointed out by Howard and Hohs,[2] but it has not yet been thoroughly investigated.

In order to investigate the detailed structure of the critical boundary, one needs accurate information regarding the reconnection processes. In this paper, we study the details of the reconnection processes in the quadratic twist map and propose a theoretical method to determine the reconnection thresholds. We show that the reversibility and symmetry of the mapping guarantee the existence of the "indicator points" in the phase space. These enable us to study the reconnection processes systematically. For twin-chains of period one and period two, the reconnection thresholds have already been determined, either exactly or approximately.[2),3)] The method presented here reproduces results which have been previously obtained, and it provides general conditions for the reconnection thresholds.

The quadratic twist map (QTM) is defined by

$$T : \begin{cases} \theta_{n+1} = \theta_n + f_\mu(I_{n+1}), \\ I_{n+1} = I_n - K\sin(\theta_n), \end{cases} \tag{1·1}$$

$$f_\mu(I) = 2\pi\mu - I^2, \tag{1·2}$$

where K represents the strength of the perturbation and μ the maximum value of the twist function $f_\mu(I)$. As the variable θ is 2π-periodic, μ is also periodic with period 1. Moreover, Eq. (1·1) is invariant under the transformation $(K, I) \mapsto (-K, -I)$. Thus it is sufficient for us to consider the parameter regions $\mu \in [-0.5, 0.5)$ and $K \in [0, \infty]$.

The mapping Eq. (1·1) is often called the logistic twist map or the standard nontwist map, depending on the form of the twist function $f_\mu(I)$.[2)-5)] In this paper, we adopt a form of Eq. (1·2) for which the twist condition

$$\frac{df_\mu(I)}{dI} \neq 0 \quad \text{for } {}^\forall I \tag{1·3}$$

fails at $I = 0$ for any value of μ in the integrable limit ($K = 0$) and for which the parameter μ itself represents the maximum value of $f_\mu(I)$.

This paper is organized as follows. In §2, we derive the location of the indicator points which play an important role in studying the reconnection processes in the QTM and give a review of the previous results on the transition to global chaos. In §3, the reconnection processes of even-periodic twin-chains are studied by using the indicator points. The reconnection thresholds are analytically derived, and a new type of reconnection process is analyzed. In §4, we focus on the reconnection processes of odd-periodic twin-chains, and a new numerical method to determine the reconnection thresholds is proposed. Section 5 contains a summary and discussion.

§2. The indicator points of the QTM

By reversibility, the QTM can be rewritten as $T = M_2 M_1$, where M_1 and M_2 are given by

$$M_1 : \begin{cases} \theta' = -\theta, \\ I' = I - K\sin(\theta), \end{cases} \tag{2·1}$$

$$M_2 : \begin{cases} \theta' = -\theta + 2\pi\mu - I^2, \\ I' = I, \end{cases} \tag{2·2}$$

and they satisfy $M_1^2 = M_2^2 = 1$. Moreover, the mapping T commutes with the mapping S (i.e., $ST = TS$) defined by

$$S : \begin{cases} \theta' = \theta + \pi, \\ I' = -I. \end{cases} \tag{2·3}$$

Previously,[6)] we showed that when there exists only one shearless curve in the phase space, it is an invariant set of both the mapping T and the mapping S. As shown in Appendix A, the invariant sets are given by the following sets $\mathcal{I}_j$ $(j = 1, 2)$:

$$\mathcal{I}_j = \bigcup_{m=-\infty}^{\infty} \{T^n \boldsymbol{x}_j^{(m)}\}_{n=0}^{\infty}, \quad (j = 1, 2) \tag{2·4}$$

where $\boldsymbol{x}_1^{(m)}$ and $\boldsymbol{x}_2^{(m)}$ are the solutions of

$$M_1 \boldsymbol{x} = R^m S \boldsymbol{x} \tag{2·5}$$

and

$$M_2\boldsymbol{x} = R^m S\boldsymbol{x}, \tag{2·6}$$

respectively. Here m represents an arbitrary integer, and R represents the linear transformation defined by

$$R\begin{bmatrix}\theta\\ I\end{bmatrix} = \begin{bmatrix}\theta - 2\pi\\ I\end{bmatrix}. \tag{2·7}$$

The solutions of Eqs. (2·5) and (2·6) are as follows:

$$\boldsymbol{x}_1^{(m)} = \begin{bmatrix}\theta_1^{(m)}\\ I_1^{(m)}\end{bmatrix} = \begin{bmatrix}\frac{1}{2}\pi(2m-1)\\ (-1)^{m+1}\ \frac{1}{2}K\end{bmatrix}, \tag{2·8}$$

$$\boldsymbol{x}_2^{(m)} = \begin{bmatrix}\theta_2^{(m)}\\ I_2^{(m)}\end{bmatrix} = \begin{bmatrix}\pi\mu + \frac{1}{2}\pi(2m-1)\\ 0\end{bmatrix}. \tag{2·9}$$

Note that $\boldsymbol{x}_1^{(m)}$ depends only on K, while $\boldsymbol{x}_2^{(m)}$ depends only on μ. If we use the 2π-periodicity of the variable θ in the interval $(-\pi, \pi]$, it is sufficient to consider only two terms ($m = 0$ and $m = 1$) in Eq. (2·4). We shall call these points, $\boldsymbol{x}_j^{(m)}$ ($j = 1, 2$), the "indicator points" in the present paper. As will be shown in what follows, we can detect the occurrence of the transition to global chaos and of the reconnection of twin-chains by investigating the iterates of the indicator points.

When the iterates of the indicator points $\boldsymbol{x}_j^{(m)}$ are confined in a bounded region, the following two cases are possible: i) they are confined on a shearless curve (see Fig. 1(a)), or ii) they are not confined on a certain KAM curve, but several robust KAM curves surrounding them prevent global chaotic motion (see Fig. 1(b)). In either case, one can say that the bounded motion of the iterates of $\boldsymbol{x}_j^{(m)}$ ensures the existence of KAM curves. On the other hand, the unbounded motion of the iterates of $\boldsymbol{x}_j^{(m)}$ guarantees the non-existence of KAM curves.

As reported in Ref. 6), we have numerically determined whether the iterates of $\boldsymbol{x}_j^{(m)}$ are bounded or not for each set of μ and K. The phase diagram so obtained is shown in Fig. 2, where the iterates of $\boldsymbol{x}_j^{(m)}$ are bounded in the gray region, but unbounded in the white region. Thus, the boundary between the gray and the white regions displayed in Fig. 2 determines the critical boundary, where the transition to global chaos occurs. In numerical calculations, we consider iterates to be bounded when the absolute values of their I components do not exceed 2 during 10^5 steps of iteration (i.e., $|I_n| < 2$ for $^\forall n \leq 10^5$). These conditions are sufficient to detect the bounded motion, because the robust KAM curves are always localized around the indicator points $\boldsymbol{x}_j^{(m)}$, as shown in Figs. 1(a) and (b).

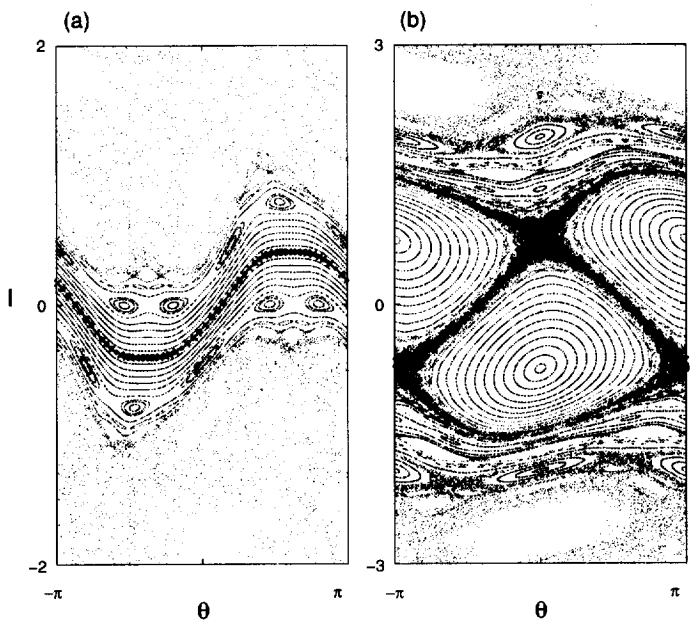

Fig. 1. Two types of bounded motions. (a) $(\mu, K) = (-0.366328694, 0.80)$, (b) $(\mu, K) = (0.089259, 0.28)$. In both figures, 50 successive iterates of $\boldsymbol{x}_1^{(1)}$ and $\boldsymbol{x}_2^{(0)}$ under the mapping T are plotted by solid circles (•) and crosses (×), respectively.

§3. Annihilation and reconnection of even-periodic twin-chains

In this section, we consider the case where either $\boldsymbol{x}_1^{(m)}$ or $\boldsymbol{x}_2^{(m)}$ is an even-periodic point with rotation number P/Q, i.e.,

$$R^P T^Q \boldsymbol{x}_j^{(m)} = \boldsymbol{x}_j^{(m)}, \quad (j = 1, 2;\ m \in Z) \tag{3·1}$$

where P and Q are relatively prime integers and let Q be even. By the symmetry of the mapping, Eq. (3·1) is reduced to more simple forms (see Appendix B):

$$T^{Q/2} \boldsymbol{x}_1^{(m)} = \boldsymbol{x}_1^{(m+P)} \tag{3·2}$$

and

$$T^{-Q/2} \boldsymbol{x}_2^{(m)} = \boldsymbol{x}_2^{(m-P)}. \tag{3·3}$$

By solving Eqs. (3·2) and (3·3), one can obtain two independent relations between μ and K parametrized by P and Q. Note that these relations do not depend on m at all. The exact iterates of $\boldsymbol{x}_1^{(m)}$ and $\boldsymbol{x}_2^{(m)}$ are given for $Q = 2, 4, 6$ and 8 in Appendix C. The obtained μ-K relations are summarized in Table I, where we put

$$\xi(\mu, K) = 1 + 2\cos\left(2\pi\mu - \frac{1}{4}K^2\right) \tag{3·4}$$

and

$$\eta(\mu, K) = 1 + \frac{\cos(3\pi\mu - K^2\cos^2(\pi\mu))}{\cos(\pi\mu)}. \tag{3·5}$$

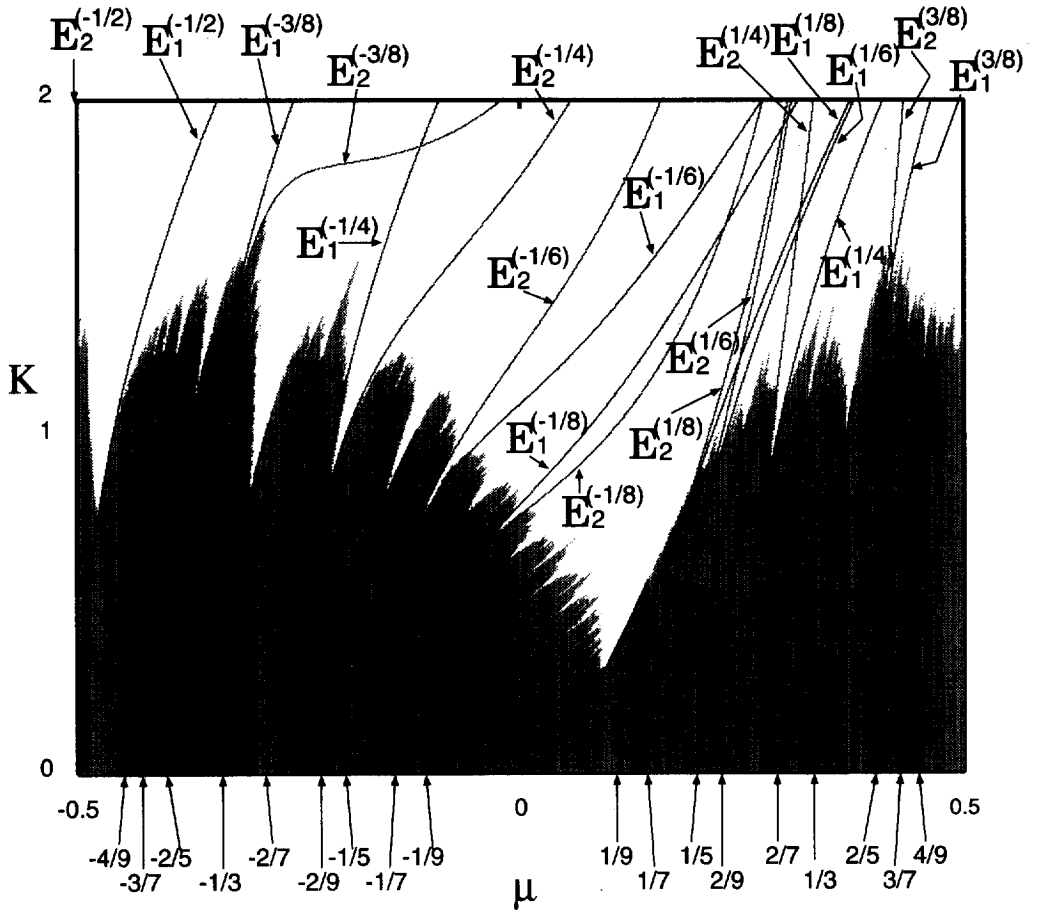

Fig. 2. Phase diagram of the quadratic twist map. The iterates of the indicator points $\boldsymbol{x}_j^{(m)}$ are bounded in the gray region but unbounded in the white region. The boundary between the gray and the white regions corresponds to the critical boundary, where the transition to global chaos occurs. The solid lines represent the (P/Q)-curves for even-periodic twin-chains with period $Q \leq 8$ and the reconnection thresholds for odd-periodic twin-chains with period $Q \leq 9$.

Table I. The μ-K relations derived from Eqs. (3·2) and (3·3).

Q	P	The μ-K relation obtained from $R^P T^Q \boldsymbol{x}_1^{(m)} = \boldsymbol{x}_1^{(m)}$	The μ-K relation obtained from $R^P T^Q \boldsymbol{x}_2^{(m)} = \boldsymbol{x}_2^{(m)}$
2	-1	$8\pi(\mu - P/Q) = K^2$	$\mu = -1/2$
4	± 1	$8\pi(\mu - P/Q) = K^2$	$4\pi(\mu - P/Q) = K^2 \cos^2(\pi\mu)$
6	± 1	$24\pi(\mu - P/Q) = K^2(2 + \xi(\mu, K)^2)$	$3\pi(\mu - P/Q) = K^2 \cos^2(\pi\mu)$
8	$\pm 3, \pm 1$	$16\pi(\mu - P/Q) = K^2(1 + \xi(\mu, K)^2)$	$8\pi(\mu - P/Q) = K^2 \cos^2(\pi\mu)(2 + \eta(\mu, K)^2)$

Let us denote the μ-K relations derived from Eqs. (3·2) and (3·3) by $E_1^{(P/Q)}$ and $E_2^{(P/Q)}$ respectively; i.e.,

$$E_j^{(P/Q)} = \{(\mu, K) \mid \hat{T}_{P,Q}\, \boldsymbol{x}_j^{(m)} = \boldsymbol{x}_j^{(m)}\}, \quad (j = 1, 2) \tag{3·6}$$

where m is an arbitrary integer and

$$\hat{T}_{P,Q} = R^P T^Q. \tag{3·7}$$

In the μ-K parameter space, the two sets $E_1^{(P/Q)}$ and $E_2^{(P/Q)}$ are described by two different curves which pass through the trivial point $(\mu, K) = (P/Q, 0)$. These curves are shown by solid lines in Fig. 2 for several values of P/Q (those for $Q \leq 8$). There are two types of characteristic μ-K curves given for each value of P/Q. We shall call these curves the right (P/Q)-curve or the left (P/Q)-curve, depending on their relative positions, corresponding to the right-hand side or the left-hand side in Fig. 2. For (P/Q)-curves that have a crossing point, we only apply the notion of right and left below the crossing point. Some of the right and the left (P/Q)-curves are summarized in Table II.

Table II. The relative location of the two curves corresponding to $E_1^{(P/Q)}$ and $E_2^{(P/Q)}$.

Q	P	left	right
2	−1	E_2	E_1
4	−1	E_1	E_2
	+1	E_2	E_1
6	−1	E_2	E_1
	+1	E_2	E_1
8	−3	E_1	E_2
	−1	E_1	E_2
	+1	E_2	E_1
	+3	E_2	E_1

Note that the (P/Q)-curves are quite similar to the (P/Q)-bifurcation curve introduced by del-Castillo-Negrete et al.,[4] where the (P/Q)-bifurcation curve is defined as the μ-K locus which represents the creation/annihilation points of the twin-chains with rotation number P/Q. It will be shown later that either the right or the left (P/Q)-curve which we have introduced here coincides well with the P/Q-bifurcation curve.

From numerical calculations, we can find the following general characteristics of the iterates of the indicator points $\boldsymbol{x}_j^{(m)}$ and the characteristic $E_j^{(P/Q)}$ curves defined by Eq. (3·6):

(i) For the μ-K parameter values given by $E_1^{(P/Q)}$(or $E_2^{(P/Q)}$), successive iterates of $\boldsymbol{x}_2^{(m)}$(or $\boldsymbol{x}_1^{(m)}$) converge to a periodic point with rotation number P/Q under the mapping $\hat{T}_{P,Q}$.

(ii) For the μ-K parameter region between the right and the left (P/Q)-curves, successive iterates of both $\boldsymbol{x}_1^{(m)}$ and $\boldsymbol{x}_2^{(m)}$ converge to an unstable periodic point with rotation number P/Q under the mapping $\hat{T}_{P,Q}$.

These properties are numerically illustrated in Fig. 3 for the case of $P/Q = -1/2$.

It is found in many cases that twin-chains with rotation number P/Q (hereafter referred to as (P/Q)-twin-chains) are created or annihilated at parameter values on the left (P/Q)-curve, and that the reconnection of the (P/Q)-twin-chains takes place at parameter values on the right (P/Q)-curve. Thus, the left (P/Q)-curve and the right (P/Q)-curve correspond to the annihilation threshold and the reconnection threshold, respectively. In Fig. 2, we can see nice agreement of the critical boundary and the right (P/Q)-curves for many P/Q. This is more clearly shown in Fig. 4 for the case of $P/Q = -1/4$. However, this correspondence does not always hold for all P/Q. For instance, in the cases of $P/Q = -1/6$ and $P/Q = -1/8$, it is the left

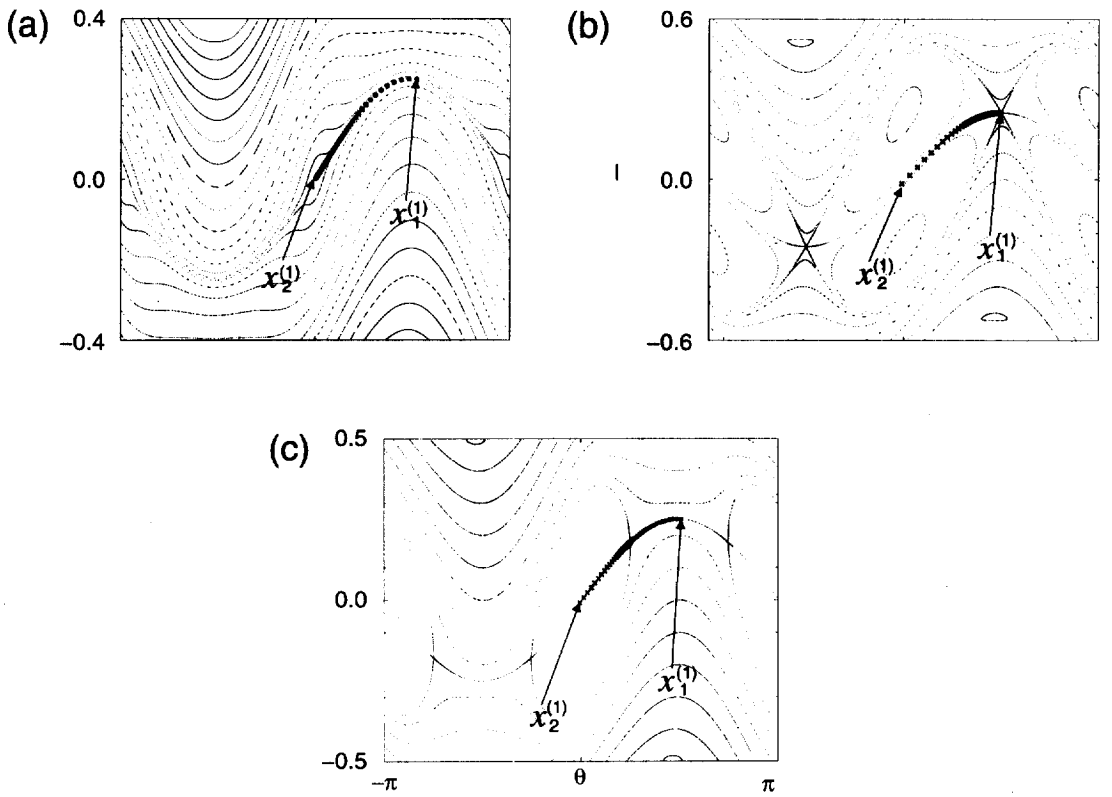

Fig. 3. Phase space portraits and successive iterates of $\boldsymbol{x}_1^{(1)}$ and $\boldsymbol{x}_2^{(1)}$ under the mapping $\hat{T}_{-1,2} = R^{-1}T^2$, where solid circles (•) represent the iterates of $\boldsymbol{x}_1^{(1)}$, and crosses (×) represent those of $\boldsymbol{x}_2^{(1)}$. (a) At $(\mu, K) = (-0.5, 0.5) \in E_2^{(P/Q)}$, $x_2^{(1)}$ is a marginally stable periodic point, and successive iterates of $x_1^{(1)}$ converge to $x_2^{(1)}$ under the mapping $\hat{T}_{-1,2}$. (b) At $(\mu, K) = (-0.490052816, 0.5) \in E_1^{(P/Q)}$, $x_1^{(1)}$ is an unstable periodic point, and successive iterates of $x_2^{(1)}$ converge to $x_1^{(1)}$ under the mapping $\hat{T}_{-1,2}$. (c) At $(\mu, K) = (-0.495, 0.5)$, successive iterates of both $x_1^{(1)}$ and $x_2^{(1)}$ converge to an unstable periodic point under the mapping $\hat{T}_{-1,2}$.

(P/Q)-curve that coincides with the critical boundary. This is more clearly shown in Fig. 5 for the case of $P/Q = -1/8$. This exceptional correspondence occurs when the left (P/Q)-curve changes to correspond to the reconnection threshold at a certain point on the curve.

Let us illustrate this for the left $(-1/8)$-curve. Figures 6(a) ∼ (e) display phase space portraits for various values of K, where K increases along the left $(-1/8)$-curve. At $K = 0.5$, marginally stable periodic points with rotation number $-1/8$ exist in the phase space, as shown in Fig. 6(a). At $K = K_1 \simeq 0.519$, the periodic point becomes unstable and gives birth to two elliptic points, as shown in Fig. 6(b). We refer to the chain of these periodic points as the primary chain. At $K = K_2 \simeq 0.5492$, another pair of periodic points with rotation number $-1/8$ is created on both sides of the primary chain via a saddle-node (SN) bifurcation. Figure 6(c) exhibits the phase space portrait at $K = 0.552$, where two chains of SN pairs appear, in addition

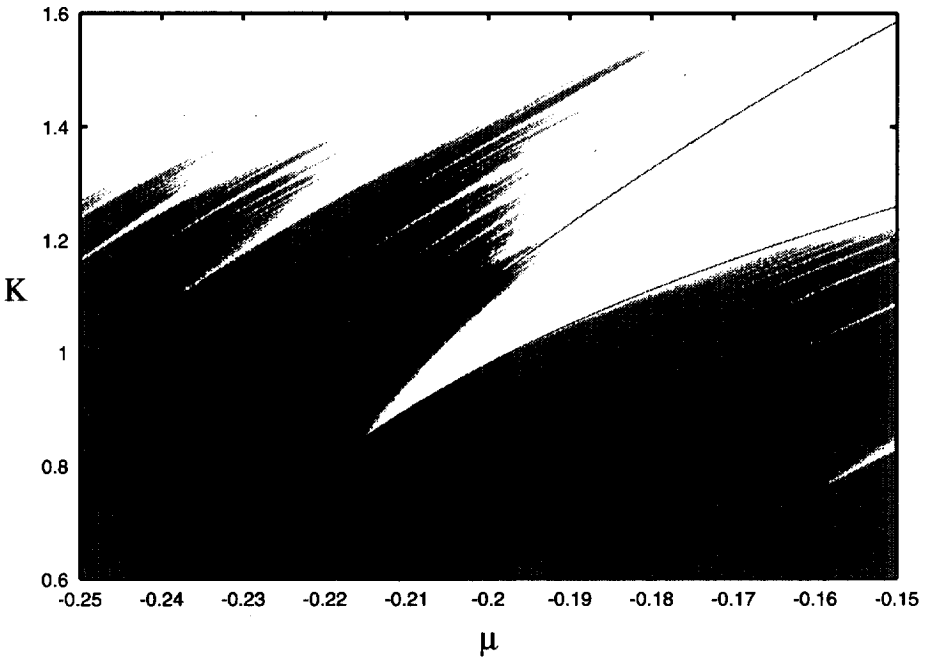

Fig. 4. Magnification of the phase diagram and the right and left $(-1/4)$-curves.

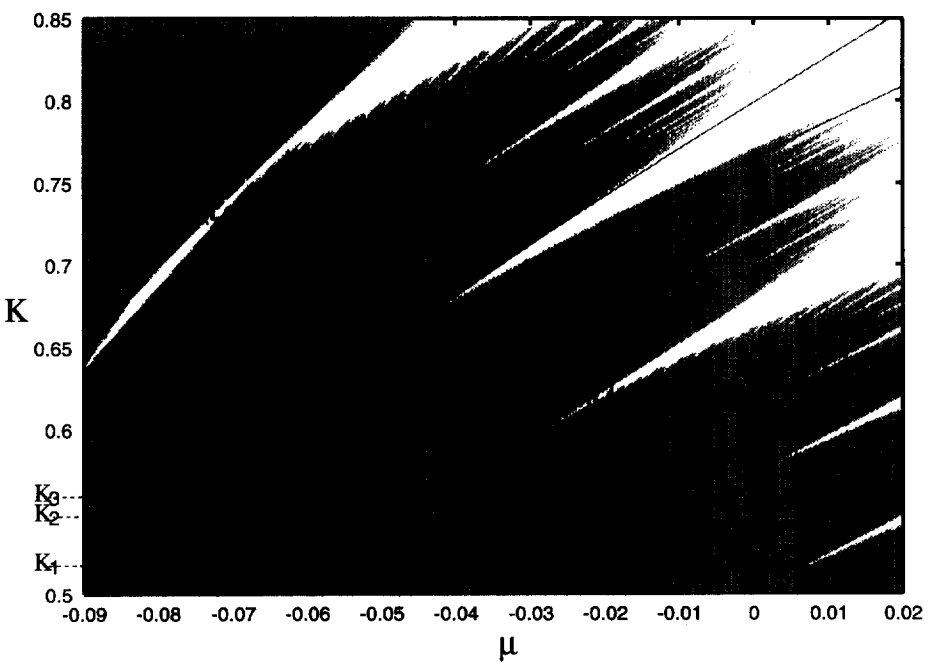

Fig. 5. Magnification of the phase diagram and the right and left $(-1/8)$-curves.

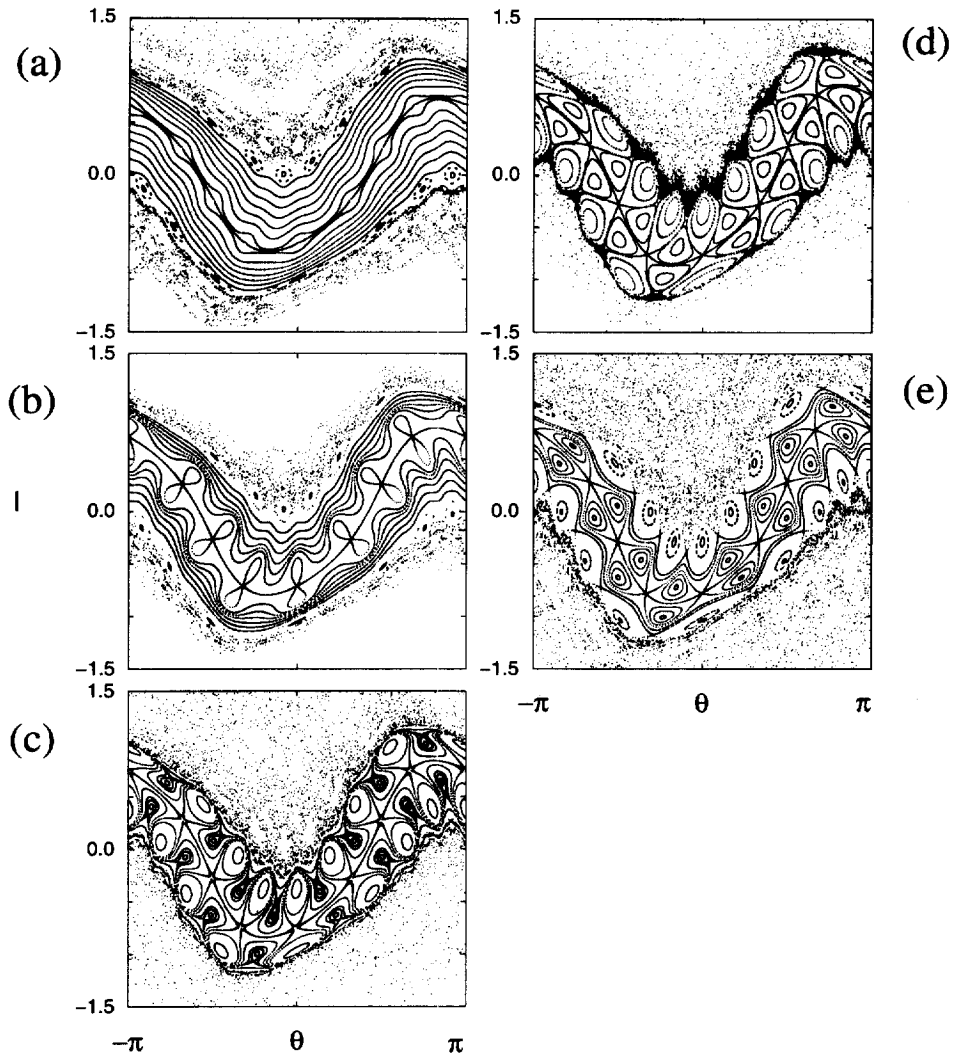

Fig. 6. The reconnection process of the primary and secondary chains with rotation number $P/Q = -1/8$. The values of μ and K increase along the left $(-1/8)$-curve as follows: (a) $(\mu, K) = (-0.084975, 0.50)$, (b) $(\mu, K) = (-0.079063, 0.53)$, (c) $(\mu, K) = (-0.074355, 0.552)$, (d) $(\mu, K) = (-0.072334, 0.561)$, (e) $(\mu, K) = (-0.070258, 0.57)$.

to the primary chain mentioned above. We refer to these chains of SN pairs as the secondary chains. Moreover, at $K = K_3 \simeq 0.561$, the two separatrices of the primary chain and those of the secondary chains merge, as shown in Fig. 6(d). As a result of the reconnection process induced by the merging of the primary and secondary chains, vortex pairs and two Poincaré-Birkhoff chains come to appear, as shown in Fig. 6(e).

To summarize, the left $(-1/8)$-curve corresponds to the annihilation threshold of the primary chain for $K < K_1$. While, for $K > K_3$, it corresponds to the

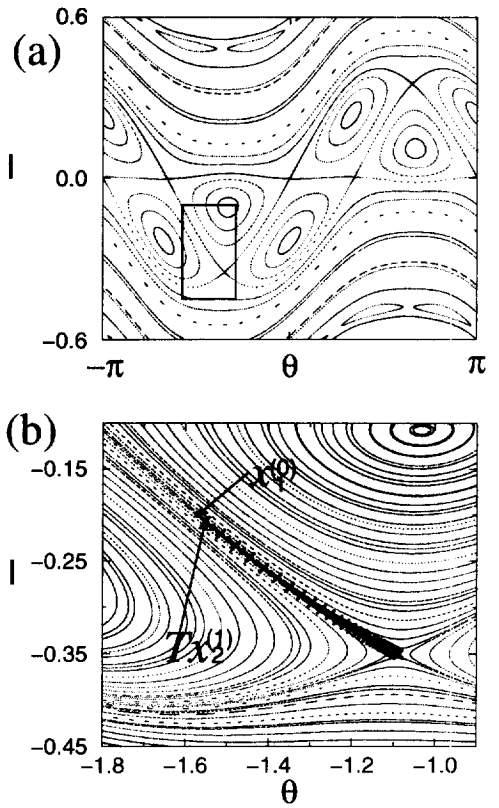

Fig. 7. (a) Phase space portraits of the $(-1/3)$-twin-chains at a reconnection threshold $(\mu, K) = (-0.32681945, 0.4)$. (b) Magnification of the box in Fig. 7(a). 90 successive iterates of $\boldsymbol{x}_1^{(0)}$ and $T\,\boldsymbol{x}_2^{(1)}$ under the mapping $\hat{T}_{-1,3}$ are also shown as solid circles (•) and crosses (×), respectively.

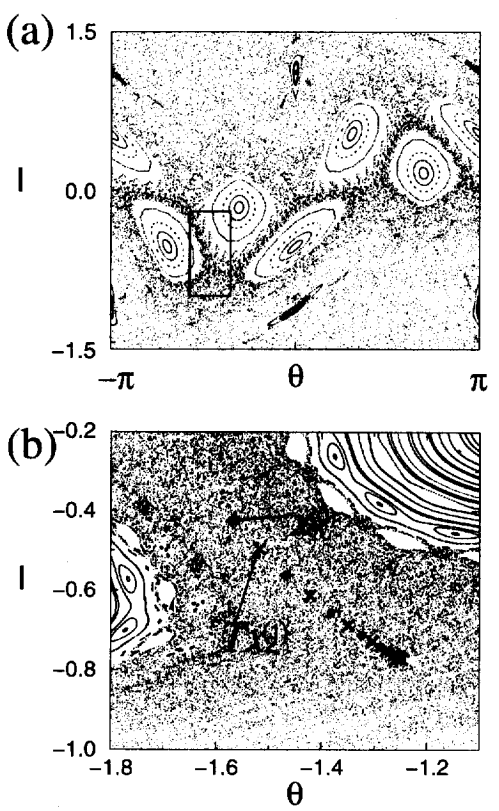

Fig. 8. (a) Phase space portraits of the $(-1/3)$-twin-chains at a reconnection threshold $(\mu, K) = (-0.30159859, 0.85)$. (b) Magnification of the box in Fig. 8(a). 12 successive iterates of $\boldsymbol{x}_1^{(0)}$ and $T\,\boldsymbol{x}_2^{(1)}$ under the mapping $\hat{T}_{-1,3}$ are also shown as solid circles (•) and crosses (×), respectively.

reconnection threshold of the vortex pairs that are formed via the reconnection process of the primary and secondary chains.

§4. Reconnection of odd-periodic twin-chains

In this section we characterize the reconnection of odd-periodic twin-chains by using the indicator points. At a reconnection threshold of the (P/Q)-twin-chains, successive iterates of both $\boldsymbol{x}_1^{(m+P)}$ and $T^{\frac{Q-1}{2}}\boldsymbol{x}_2^{(m)}$ approach the same hyperbolic periodic point of the reconnecting twin-chains under the mapping $\hat{T}_{P,Q}$. Figure 7(a) corresponds to the case of the $(-1/3)$-twin-chains at the reconnection threshold. Figure 7(b) is the magnification of the phase space near the lower hyperbolic periodic

point of the $(-1/3)$-twin-chains, where $\hat{T}^n_{-1,3}\,\boldsymbol{x}_1^{(0)}$ and $\hat{T}^n_{-1,3}\,T^1\boldsymbol{x}_2^{(1)}$ approach the same hyperbolic periodic point as n increases. We have numerically confirmed this property for all odd-periodic twin-chains with period $Q \leq 9$. This property seems to hold even at a large K-value, as shown in Fig. 8, where we can still observe monotonic convergence in spite of strong chaos around a hyperbolic periodic point.

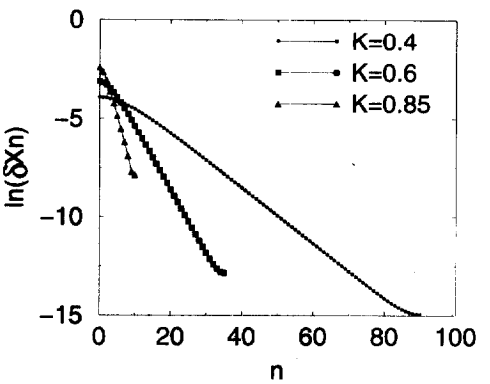

Fig. 9. Numerical evidence for the exponential decrease of δX_n at a reconnection threshold for $K = 0.4$, $K = 0.6$ and $K = 0.85$.

Consider the quantity δX_n given by

$$\delta X_n = || \hat{T}^n_{P,Q}\,\boldsymbol{x}_1^{(m+P)} - \hat{T}^n_{P,Q}\,T^{\frac{Q-1}{2}}\boldsymbol{x}_2^{(m)}||, \quad (4\cdot1)$$

where m is an arbitrary integer and $||\cdot||$ represents the Euclidian norm. At the reconnection threshold, δX_n is expected to decrease exponentially as

$$\delta X_n \propto \lambda^n, \quad (4\cdot2)$$

where λ represents the smaller (stable) eigenvalue of the tangent map of the mapping T^Q evaluated at the hyperbolic periodic point of the (P/Q)-twin-chains. Numerical evidence for the exponential scaling regime of Eq. (4·2) at the reconnection threshold of the $(-1/3)$-twin-chains is shown in Fig. 9 for various K-values. There appear large deviations from the scaling regime when the number of iterations n becomes extremely large, because the monotonic convergence of δX_n is violated by heteroclinic chaos near the hyperbolic periodic point. However, as shown in Table III, the decay rates in the scaling regime are in good agreement with the theoretically estimated values of $\ln(\lambda)$.

Table III. Slopes of the scaling regime in Fig. 9 and theoretically estimated values of $\ln(\lambda)$.

K	slope	$\ln(\lambda)$
0.40	−0.140	−0.142
0.60	−0.320	−0.325
0.85	−0.640	−0.668

On the basis of the remarkable convergent property mentioned above, the determination of the reconnection threshold is reduced to the problem of finding the parameter values where $\delta X_N \leq \epsilon$ holds for a given small value ϵ with a certain large N. The merit of this computational criterion is that it does not require any additional knowledge about the detailed structure of twin-chains, such as the location of the periodic point and its stability. Applying this criterion, we numerically determined the reconnection thresholds for odd-periodic twin-chains with the period $Q \leq 9$, which are indicated by solid lines for $Q =$ odd in Fig. 2. The results based on the above technique seem to reproduce the reconnection thresholds. This is illustrated more clearly in Fig. 10 for the case of the $(-1/3)$-twin-chains.

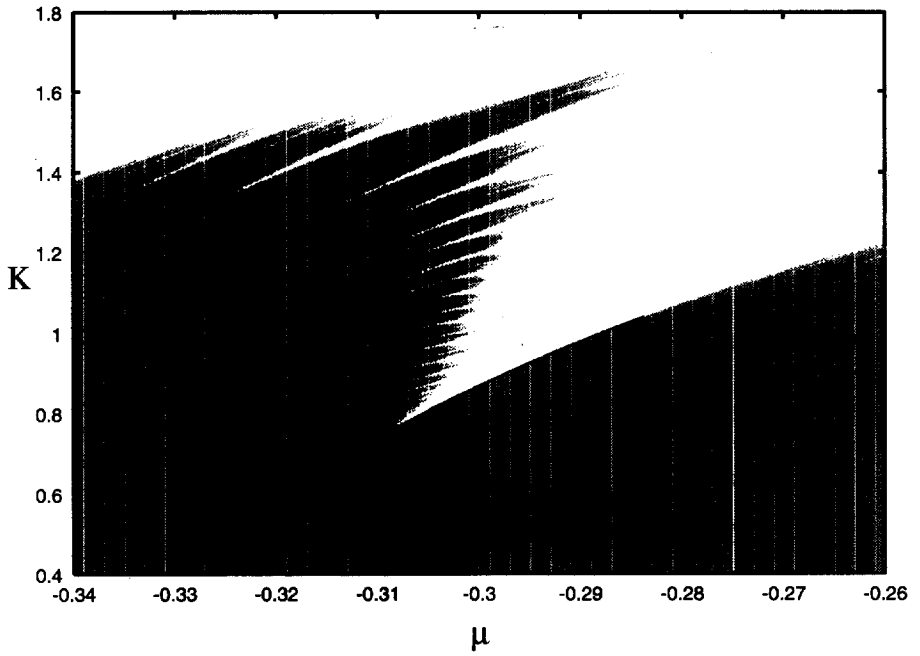

Fig. 10. Magnification of the phase diagram and the reconnection threshold for the $(-1/3)$-twin-chains.

§5. Summary and discussion

We have studied in detail the reconnection processes of twin-chains in the QTM by investigating the iterates of the indicator points $\boldsymbol{x}_j^{(m)}$ which belong to the invariant sets of both the mapping T and the mapping S. For the case of even-periodic twin-chains, we introduced (P/Q)-curves in the parameter space, on which either the annihilation or the reconnection of the (P/Q)-twin-chains occurs. We succeeded in deriving the (P/Q)-curves analytically for $Q \leq 8$. One can also derive (P/Q)-curves with larger value of Q by solving Eqs. (3·2) and (3.3). On the other hand, for the case of odd-periodic twin-chains, we propose a numerical method to determine the reconnection threshold. The method is based on the observation that the successive iterates of the indicator points converge to the same hyperbolic periodic point at the reconnection threshold. Numerical results clearly show that the critical boundary is described well by the reconnection thresholds of twin-chains.

Finally, we briefly discuss the reconnection process between the primary and the secondary twin-chains which was found for the $(-1/8)$-twin-chains. The variety of reconnecting twin-chains has been studied in cubic and quartic twist maps.[3] For example, cubic twist maps exhibit the reconnection of three island chains with the same rotation number. This is a natural consequence of the fact that the cubic twist function generically has two extrema and that each extremum generates an inherent reconnection process. However, it is surprising that multiple reconnection processes occur simultaneously even in the QTM whose twist function has only one

extremum. The occurrence of the secondary twin-chains inevitably ensures the existence of multiple shearless curves in the phase space, neither of which passes through the indicator points $\boldsymbol{x}_j^{(m)}$(see Figs. 6(c) and (e)). Our result suggests that shearless curves can be created by nonintegrable nonlinear perturbations. This problem will be discussed elsewhere.

Appendix A
—— *The Invariant Sets $\mathcal{I}_j$ $(j = 1, 2)$* ——

It is trivial to show that $\mathcal{I}_j$ $(j = 1, 2)$ given by Eq. (2·4) is an invariant set of T. Here we show that $\mathcal{I}_j$ is invariant under the transformation S, i.e., $S\mathcal{I}_j = \mathcal{I}_j$ $(j = 1, 2)$. In order to do this, we show that $ST^n\boldsymbol{x}_j^{(m)}$ is also an element of $\mathcal{I}_j$ as follows:

$$\begin{aligned} ST^n\boldsymbol{x}_1^{(m)} &= T^nS\boldsymbol{x}_1^{(m)} = T^nR^{-m}M_1\boldsymbol{x}_1^{(m)} = T^nM_1\boldsymbol{x}_1^{(3m)} \\ &= T^{n-1}M_2\boldsymbol{x}_1^{(3m)} = T^n\boldsymbol{x}_1^{(1-3m)}, \end{aligned} \tag{A·1}$$

$$\begin{aligned} ST^n\boldsymbol{x}_2^{(m)} &= T^nS\boldsymbol{x}_2^{(m)} = T^nR^{-m}M_2\boldsymbol{x}_2^{(m)} = T^nM_2\boldsymbol{x}_2^{(3m)} \\ &= T^{n+1}M_1\boldsymbol{x}_2^{(3m)} = T^n\boldsymbol{x}_2^{(1-3m)}, \end{aligned} \tag{A·2}$$

where we have used the relation $ST = TS$ in the first equalities, and Eqs. (2·5) and (2·6) in the second equalities. Moreover, we use the following relations in the last equalities:

$$M_2\boldsymbol{x}_1^{(m)} = T\boldsymbol{x}_1^{(1-m)}, \tag{A·3}$$

$$M_1\boldsymbol{x}_2^{(m)} = T^{-1}\boldsymbol{x}_2^{(1-m)}. \tag{A·4}$$

Appendix B
—— *Derivation of Eqs. (3·2) and (3·3)* ——

Assume that $\boldsymbol{x}_j^{(m)}$ $(j = 1, 2;\ m \in Z)$ given by Eqs. (2·8) and (2·9) are even-periodic points with rotation number P/Q; i.e.,

$$R^PT^Q\boldsymbol{x}_j^{(m)} = \boldsymbol{x}_j^{(m)}. \quad (j = 1, 2) \tag{B·1}$$

The property of the involutions M_1 and M_2 implies

$$M_1T^{Q/2} = T^{-Q/2}M_1, \quad M_2T^{-Q/2} = T^{Q/2}M_2. \tag{B·2}$$

Therefore we have

$$M_1T^{Q/2}\boldsymbol{x}_1^{(m)} = T^{-Q/2}M_1\boldsymbol{x}_1^{(m)} = T^{-Q/2}R^mS\boldsymbol{x}_1^{(m)} = R^mST^{-Q/2}\boldsymbol{x}_1^{(m)} \tag{B·3}$$

and

$$M_2T^{-Q/2}\boldsymbol{x}_2^{(m)} = T^{Q/2}M_2\boldsymbol{x}_2^{(m)} = T^{Q/2}R^mS\boldsymbol{x}_2^{(m)} = R^mST^{Q/2}\boldsymbol{x}_2^{(m)}, \tag{B·4}$$

where we have used Eqs. (2·5) and (2·6) in the second equalities and the relation $ST = TS$ in the third equalities.

On the other hand, Eq. (B·1) implies

$$T^{-Q/2}\boldsymbol{x}_j^{(m)} = R^P T^{Q/2}\boldsymbol{x}_j^{(m)}, \quad (j = 1, 2) \tag{B·5}$$

$$T^{Q/2}\boldsymbol{x}_j^{(m)} = R^{-P} T^{-Q/2}\boldsymbol{x}_j^{(m)}. \quad (j = 1, 2) \tag{B·6}$$

Substituting (B·5) and (B·6) into (B·3) and (B·4), respectively, we have

$$M_1 T^{Q/2}\boldsymbol{x}_1^{(m)} = R^{m+P} S T^{Q/2}\boldsymbol{x}_1^{(m)} \tag{B·7}$$

and

$$M_2 T^{-Q/2}\boldsymbol{x}_2^{(m)} = R^{m-P} S T^{-Q/2}\boldsymbol{x}_2^{(m)}. \tag{B·8}$$

Since these equations are equivalent to Eqs. (2·5) and (2·6), the solutions are given by

$$T^{Q/2}\boldsymbol{x}_1^{(m)} = \boldsymbol{x}_1^{(m+P)}, \tag{B·9}$$

$$T^{-Q/2}\boldsymbol{x}_2^{(m)} = \boldsymbol{x}_2^{(m-P)}, \tag{B·10}$$

respectively.

Appendix C

—— *Exact Iterations of* $\boldsymbol{x}_1^{(m)}$ *and* $\boldsymbol{x}_2^{(m)}$ ——

The exact expressions for $T^n\boldsymbol{x}_1^{(m)}$ $(n = 0, \pm 1, \pm 2)$ are given by

$$T^{-2}\boldsymbol{x}_1^{(m)} = \begin{bmatrix} \frac{\pi}{2}(2m-1) - 4\pi\mu + \frac{1}{4}K^2(1+\xi(\mu,K)^2) \\ (-1)^{m+1}\frac{1}{2}K\{\xi(\mu,K) + 2\cos(4\pi\mu - \frac{1}{4}K^2(1+\xi(\mu,K)^2))\} \end{bmatrix}, \tag{C·1}$$

$$T^{-1}\boldsymbol{x}_1^{(m)} = \begin{bmatrix} \frac{\pi}{2}(2m-1) - 2\pi\mu + \frac{1}{4}K^2 \\ (-1)^{m+1}\frac{1}{2}K\xi(\mu,K) \end{bmatrix}, \tag{C·2}$$

$$\boldsymbol{x}_1^{(m)} = \begin{bmatrix} \frac{\pi}{2}(2m-1) \\ (-1)^{m+1}\frac{1}{2}K \end{bmatrix}, \tag{C·3}$$

$$T\boldsymbol{x}_1^{(m)} = \begin{bmatrix} \frac{\pi}{2}(2m-1) + 2\pi\mu - \frac{1}{4}K^2 \\ (-1)^m\frac{1}{2}K \end{bmatrix}, \tag{C·4}$$

$$T^2\boldsymbol{x}_1^{(m)} = \begin{bmatrix} \frac{\pi}{2}(2m-1) + 4\pi\mu - \frac{1}{4}K^2(1+\xi(\mu,K)^2) \\ (-1)^m\frac{1}{2}K\xi(\mu,K) \end{bmatrix}, \tag{C·5}$$

where $\xi(\mu, K)$ is given by Eq. (3·4).

While the exact expressions for $T^n\boldsymbol{x}_2^{(m)}$ $(n = 0, \pm 1, \pm 2)$ are given by

$$T^{-2}\boldsymbol{x}_2^{(m)} = \begin{bmatrix} \frac{\pi}{2}(2m-1) - 3\pi\mu + K^2\cos^2(\pi\mu) \\ (-1)^{m+1}K\cos(\pi\mu)\eta(\mu,K) \end{bmatrix}, \tag{C·6}$$

$$T^{-1}\boldsymbol{x}_2^{(m)} = \begin{bmatrix} \frac{\pi}{2}(2m-1) - \pi\mu \\ (-1)^{m+1} K \cos(\pi\mu) \end{bmatrix}, \tag{C·7}$$

$$\boldsymbol{x}_2^{(m)} = \begin{bmatrix} \frac{\pi}{2}(2m-1) + \pi\mu \\ 0 \end{bmatrix}, \tag{C·8}$$

$$T\boldsymbol{x}_2^{(m)} = \begin{bmatrix} \frac{\pi}{2}(2m-1) + 3\pi\mu - K^2\cos^2(\pi\mu) \\ (-1)^m K \cos(\pi\mu) \end{bmatrix}, \tag{C·9}$$

$$T^2\boldsymbol{x}_2^{(m)} = \begin{bmatrix} \frac{\pi}{2}(2m-1) + 5\pi\mu - K^2\cos^2(\pi\mu)(1+\eta(\mu,K)^2) \\ (-1)^m K \cos(\pi\mu)\eta(\mu,K) \end{bmatrix}, \tag{C·10}$$

where $\eta(\mu, K)$ is given by Eq. (3·5).

References

1) *Hamiltonian Dynamical Systems*, ed. R. S. MacKay and J. D. Meiss (Adam Hilger, London, 1987).
2) J. E. Howard and S. M. Hohs, Phys. Rev. **A29** (1984), 418.
3) J. E. Howard and J. Humpherys, Physica **D80** (1995), 256.
4) D. del-Castillo-Negrete, J. M. Greene and P. J. Morrison, Physica **D91** (1996), 1.
5) D. del-Castillo-Negrete, J. M. Greene and P. J. Morrison, Physica **D100** (1997), 311.
6) S. Shinohara and Y. Aizawa, Prog. Theor. Phys. **97** (1997), 379.